6. Supplementary information

6.1 Process conditions for CRD wood pyrolysis DOE model

For analysing the influence of pyrolysis process conditions on biochar properties using response surface methodology's (RSM) central composite design (CCD), three independent variables or factors coded as A, B, C, with five levels of operation parameters coded as -α, -1, 0, 1, α, were considered as in Supplementary Figure S1. These variables were pyrolysis temperature (400-800 °C), BRT (30-90 min), and mass of CRD wood feedstock loaded into the reactor for pyrolysis (50-250 g). To have a robust representation of the design, eight factorial or corner points (p_f), six axial points (p_a), and one to three center points (p_c) could be suitable to derive adequate conclusions for a system. In fact, the number of independent variables can also be increased for a more thorough evaluation but the total number of experimental investigations will proportionally increase, thus, increasing resource utilization w.r.t feedstock, time, money, and energy. Nevertheless, this design efficiently marks important relationships between process parameters to render superior performances of the pyrolysis system.

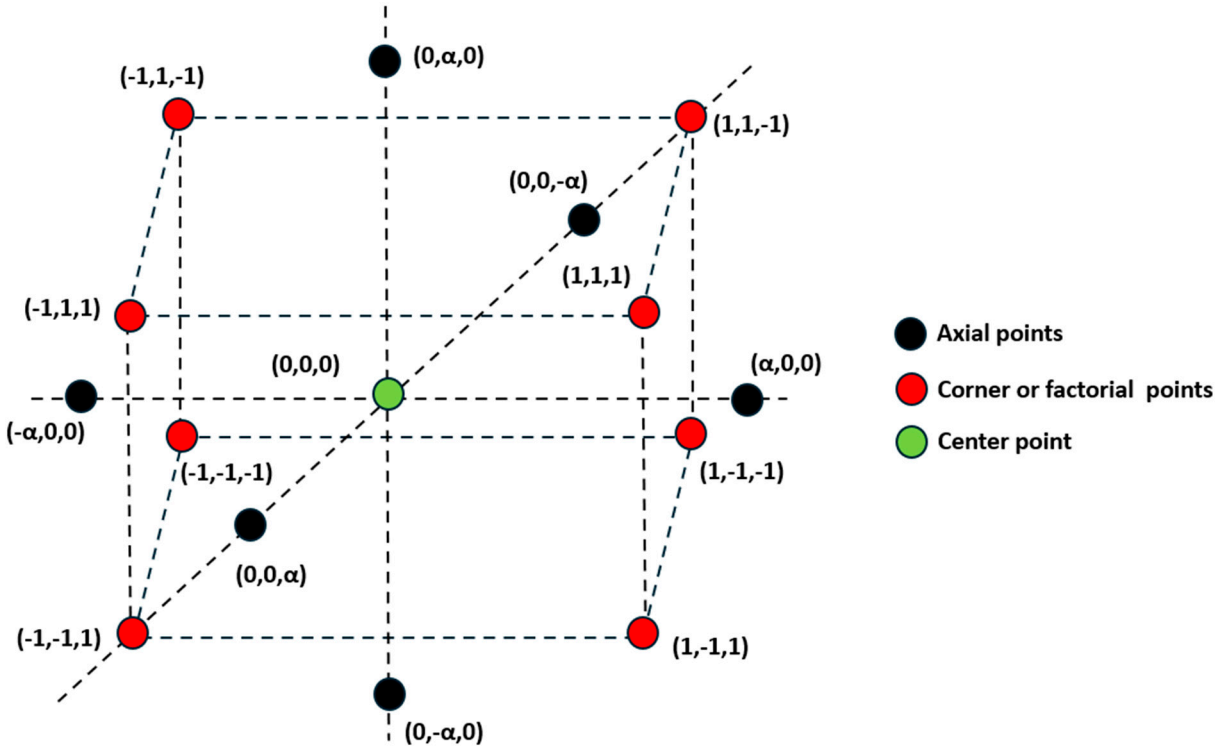

Supplementary Figure S1: RSM's CCD design points

The total number of experimental rounds to be carried out, can be determined by Supplementary Equation S1,

$$N = p_f + p_a + p_c$$

Supplementary Equation S1

This can also be written arithmetically as in Supplementary Equation S2:

$$N = 2^k + 2k + 1$$

Supplementary Equation S2

Here, 'k' represents total number of independent variables. Here, only one center point has been mentioned. More center point experiments could be run to ensure reliability. In our case, a duplicate experiment was carried out for a non-center point. The equation and total number of experiments now become:

$N = 2^3 + 2(3) + 1 = 15$

Supplementary Equation S3

The value of axial point, α, is given as in Supplementary Equation S4:

$\alpha = (2^k)^{1/4}$

Supplementary Equation S4

For three independent variables,

$\alpha = (2^3)^{\frac{1}{4}} = 1.682$

Supplementary Equation S5

An experimental design for the three independent variables can be adopted w.r.t the coded values of all five levels as shown in Supplementary Table S1.

Supplementary Table S1: Run order with coded and actual values for pyrolysis independent variables

Standard order	Run order	Coded and actual values for independent variables		
		A: Temperature (°C)	B: BRT (min)	C: Mass of feedstock (g)
11	1	400 **(-α)**	60 **(0)**	100 **(-1)**
2	2	600 **(0)**	90 **(+α)**	200 **(+1)**
16	3	600 **(0)**	30 **(-α)**	200 **(+1)**
3	4	500 **(-1)**	75 **(+1)**	200 **(+1)**
1	5	600 **(0)**	60 **(0)**	100 **(-1)**
6	6	500 **(-1)**	75 **(+1)**	150 **(0)**
13	7	500 **(-1)**	90 **(+α)**	150 **(0)**
10	8	600 **(0)**	45 **(-1)**	50 **(-α)**
5	9	700 **(+1)**	90 **(+α)**	200 **(+1)**
4	10	800 **(+α)**	75 **(+1)**	200 **(+1)**
7	11	700 **(+1)**	75 **(+1)**	200 **(+1)**
9	12	500 **(-1)**	90 **(+α)**	250 **(+α)**
8	13	600 **(0)**	90 **(+α)**	250 **(+α)**
15	14	700 **(+1)**	45 **(-1)**	150 **(0)**
14	15	400 **(-α)**	90 **(+α)**	200 **(+1)**
12	16	600 **(0)**	60 **(0)**	150 **(0)**

6.2 Statistical analysis for DOE

Supplementary Table S2: Coefficients table for DOE independent variables to evaluate their influence on the different response variables. The p-values for pyrolysis temperature (A) are <0.05 for all response variables suggesting that it has the most dominant influence on biochar properties

	Intercept	A	B	C	AB	AC	BC	A^2	B^2	C^2
Carbon	81.9567	6.2301	0.7381	1.9317						
p-values		0.0002	0.5617	0.4435						
BET surface area	230.5020	84.6827	57.4696	-23.4390	4.2486	-12.0859	-125.5880	-46.6398	10.6473	209.0550
p-values		0.0010	0.0194	0.3150	0.8474	0.7916	0.0230	0.0034	0.2764	0.0119
Volatile carbon (VC)	18.0237	-6.6995	-0.1090	0.9720						
p-values		< 0.0001	0.8912	0.5392						
Fixed carbon (FC)	75.2320	6.0109	1.2705	-0.6543						
p-values		0.0099	0.5398	0.8718						
TGA R50	0.5942	0.0371	-0.0035	-0.0226						
p-values		0.0001	0.6195	0.1190						
H/C	0.3136	-0.2017	-0.0224	0.0303	-0.0075	0.1497	0.0153			
p-values		< 0.0001	0.1099	0.1850	0.7145	0.0038	0.4522			
O/C	0.0613	-0.0829	-0.0040	0.0121	-0.0162	0.1069	0.0112			
p-values		< 0.0001	0.6894	0.4763	0.3198	0.0059	0.4779			
Thermostable fraction (TSF)	79.9473	8.1060	1.5941	-0.9558						
p-values		0.0032	0.4937	0.8336						
Micropore volume	0.1130	0.0426	0.0240	-0.0086	-0.0006	-0.0061	-0.0478	-0.0203	0.0016	0.0806
p-values		0.0004	0.0214	0.3844	0.9532	0.7546	0.0358	0.0031	0.6873	0.0184

Supplementary Table S3: Fit statistics for DOE response variables

	Carbon	BET surface area	Volatile carbon (VC)	Fixed carbon (FC)	TGA R50	H/C	O/C	Thermostable fraction (TSF)	Micropore volume
Std. Dev.	4.13	26.79	2.61	6.72	0.03	0.03	0.02	7.54	0.01
Mean	81.86	236.15	19.22	74.94	0.58	0.35	0.09	79.47	0.11
C.V. %	5.05	11.34	13.55	8.97	3.92	9.17	28.68	9.49	10.41
R^2	0.73	0.97	0.88	0.45	0.77	0.98	0.93	0.54	0.98
Adjusted R^2	0.66	0.93	0.84	0.31	0.71	0.96	0.89	0.43	0.94
Predicted R^2	0.46	0.62	0.77	0.12	0.50	0.74	0.52	0.26	0.44
Adeq Precision	11.38	15.19	17.23	6.14	11.22	31.54	17.56	7.33	16.36

6.3 Energy and efficiency calculations for biochar production in different reactor configurations – A thermal decomposition perspective

For estimating the material energy balance and performance efficiency of the two pyrolysis reactors utilized (horizontal tube furnace and rotary retort-furnace reactors) in which isobaric (all tests at constant atmospheric pressure) thermochemical conversions of CRD wood under the same temperatures, BRT, but different mass of feed (50-250 g versus 3 kg) was carried out, calculation of total energy input, energy output, net energy loss followed by pyrolyzer efficiency are important steps. Energy input is basically derived from the CRD biomass feedstock entering the reactor whereas energy output is the heat spent/lost to volatilize inbound biomass water as steam or superheated steam (gas) along with the energy value of biochar product. Equations for these calculations were referred from [25,38]. Here, energy value of biooil and pyrolysis gas were not considered because of three reasons: a) no instrumentation for gas collection and condensation (so, biooil and gas yield cannot be estimated) was used during the experiments; b) any pyrolysis gas generated was directly fed to the combustion chamber of the in-house pilot pyrolyzer via a vacuum suction pump/hose for contributing to a meagre part of its energy demand; and c) calculation of HHV for non-biochar products from pyrolysis like biooil, dust, fines, and pyrolysis gas was not possible due to absence of appropriate collection units. Since biomass conversion to biochar is mainly reliant on material heat transfer, an external metric like reactor power consumption is also not directly related to this particular thermal decomposition process.

Hence, for material energy balance calculations, only biochar was treated as the product of interest and recovered from the pyrolysis reactor. For CRD wood prior to pyrolysis, its 0.18% moisture post-drying, was considered.

Firstly, energy input is calculated using the expression:

$$Q_{input} = \text{Mass of CRD wood} \times \text{HHV of CRD wood}$$

Supplementary Equation S6

where, mass of wood is expressed as kg and its HHV as KJ/kg.

As the next part, energy output can be calculated as three separate steps. This includes loss of energy due to the necessity in evaporation of water to different phases, and energy retention in biochar produced. In the first step, energy required to remove the 0.18% water in biomass as vapor or saturated steam is calculated, i.e, as latent heat:

$$\mathrm{Q_{water,vapor}}\ (\text{or})Q_{w,v} = \mathrm{n} \times \mathrm{C_{p,v}} \times (373 - \mathrm{T_{RT}})$$

Supplementary Equation S7

Here, n is the number of moles of water in CRD biomass, $C_{p,v}$ is the specific heat capacity (C_P) of water vapor at 100 °C or 373 K expressed as (KJ/mol.K), and T_{RT} is the ambient temperature in K. The final unit of $Q_{water,vapor}$ is KJ. As the second step, energy spent to convert this vapor or steam to gas or superheated steam is calculated as:

$$\mathrm{Q_{water,gas}}\ (\text{or})Q_{w,g} = \mathrm{n} \times \mathrm{C_{p,g}} \times (\mathrm{T_{PG}} - 373)$$

Supplementary Equation S8

Here, n is the number of moles of water in CRD biomass, $C_{p,g}$ is the specific heat capacity (C_P) of water as gas derived out of the three pyrolysis rounds at 500, 700, and 800 °C expressed as (KJ/mol.K), and T_{PG} is the pyrolysis gas temperature in K. The final unit of $Q_{water,gas}$ is KJ. As the third step, energy content of biochar is calculated as:

$$\mathrm{Q_{biochar}} = \text{Yield of biochar} \times \text{HHV of biochar}$$

Supplementary Equation S9

Yield and HHV of biochar are calculated for each of the three pyrolysis rounds resulting in B500, B700, and B800. These three conditions were picked for the horizontal tube furnace reactor since all these conditions harbor the same BRT, mass of feedstock, and only vary across pyrolysis temperatures. This would facilitate easy mapping of the reactor's performance efficiencies as variations in energy requirements exist. Also, the temperature of pyrolysis gas is usually lower than the set point pyrolysis temperature mostly due to convective or radiative heat losses arising from the

reactor's design. This was the same set up used in [24] where thermal inertia did not exceed over 150 °C (upper range) for tests conducted even at 800 °C. In the horizontal rotary retort-furnace reactor set up, a 15-fold higher feed mass was utilized to check the robustness of our experimental design. Here too, thermal inertia has the same 150 °C upper range. The total energy output was then calculated as:

$$Q_{output} = Q_{water,vapor} + Q_{water,gas} + Q_{biochar}$$

Supplementary Equation S10

With this, the net energy loss is calculated using the expression:

$$Q_{net} = Q_{input} - Q_{output}$$

Supplementary Equation S11

Pyrolysis efficiency, η_{system}, can then be computed via:

$$\eta_{system} = \frac{Q_{output}}{Q_{input}} \times 100$$

Supplementary Equation S12

Variations in Q_{output} and η_{system} are observed with different degrees of thermal inertia.

For determining the pyrolyzer system's energy performance, three scenarios were considered w.r.t thermal inertia: no thermal inertia, 100 °C, and 200 °C. Heat loss through thermal inertia generally means that the set point temperature is not exactly reached by the biomass inside the reaction zone since. So, the temperature of product gas also is lowered and correlates negatively with thermal inertia. From Supplementary Table S4, the first observation is that heat loss assumptions did not have any drastic influence over η_{system}. For example, in the horizontal tube furnace and the rotary retort-furnace reactors, η_{system} dropped from about 39% to 34% and 47% to 40% commonly across all three thermal inertia classes, respectively. It is only within each category that efficiency decreased with rise in temperature. As increase in pyrolysis temperatures meant that more energy is spent to convert inherent water from the vapor or steam phase to the gas phase, increments in $Q_{w,g}$ was spotted. On the contrary, an immediate response of decrease in $Q_{w,g}$ and eventually Q_{output} were seen when heat loss faced by the reactor comes into play and superheating water vapor to that specific temperature (to match the new pyrolysis gas temperature) gets complicated – all pointing out at consequences of differences between the internal temperature faced by biomass in the retort during pyrolysis and the external furnace temperature, also termed as thermal gradient. Additionally, if the initial water content was also higher than 0.18%, more energy would be needed to drive it towards boiling point and greater will be the value of $Q_{w,v}$ too, that would belittle the concept of sensible heating. So, drying the biomass feedstock prior to pyrolysis is an unavoidable upstream step that must be followed to reduce energy consumption and overall losses in moisture handling, and prevent any delay in conversion. When calculating $Q_{biochar}$, it decreased from 1.6 MJ to 1.4 MJ and 28.6 MJ to 24.8 MJ along B500, B700, and B800 for both reactors mainly due to a reduction in yield with high pyrolysis temperatures. The yield of biochar from B500-B800 reduced from 26.9% to 21.1% and 32.1% to 26.2% for the horizontal tube furnace and rotary retort-furnace reactors, respectively. This invariably has a direct impact on the amount of energy lost during the process as waste heat (Q_{net}). In fact, for the rotary retort set up, both energy loss and efficiency can reach extremities owing to the relatively larger size of equipment and quantity of material handled.

Supplementary Table S4: Material energy balance and pyrolyzer efficiency during biomass thermal decomposition. Case 1: 0.18% internal moisture

Horizontal tube furnace reactor with feeding of CRD wood containing 0.18 wt% initial moisture								
Sample	**Pyrolysis set point temperature (K)**	**Q_{input} (KJ)**	**$Q_{water,vapor}$ (kJ)**	**$Q_{water,gas}$ (kJ)**	**$Q_{biochar}$ (kJ)**	**Q_{output} (kJ)**	**Q_{net} (kJ)**	**η_{system} (%)**
Assuming no thermal inertia during pyrolysis								
B500	**773.00**	4056.00	0.05	0.35	1601.09	1601.49	2454.51	39.48
B700	**973.00**	4056.00	0.05	0.52	1514.65	1515.22	2540.78	37.36
B800	**1073.00**	4056.00	0.05	0.62	1381.63	1382.30	2673.70	34.08
Assuming 100 °C thermal inertia during pyrolysis								
B500	**773.00**	4056.00	0.05	0.27	1601.09	1601.41	2454.59	39.48
B700	**973.00**	4056.00	0.05	0.44	1514.65	1515.14	2540.86	37.36
B800	**1073.00**	4056.00	0.05	0.52	1381.63	1382.20	2673.80	34.08
Assuming 200 °C thermal inertia during pyrolysis								
B500	**773.00**	4056.00	0.05	0.20	1601.09	1601.34	2454.66	39.48
B700	**973.00**	4056.00	0.05	0.35	1514.65	1515.05	2540.95	37.35
B800	**1073.00**	4056.00	0.05	0.44	1381.63	1382.12	2673.88	34.08
Horizontal rotary retort-furnace reactor with feeding of CRD wood containing 0.18 wt% initial moisture								
Sample	**Pyrolysis set point temperature (K)**	**Q_{input} (KJ)**	**$Q_{water,vapor}$ (KJ)**	**$Q_{water,gas}$ (KJ)**	**$Q_{biochar}$ (KJ)**	**Q_{output} (KJ)**	**Q_{net} (KJ)**	**η_{system} (%)**
Assuming no thermal inertia during pyrolysis								
B500	**773.00**	60840.00	0.79	5.32	28604.39	28610.49	32229.51	47.03
B700	**973.00**	60840.00	0.79	7.86	25859.28	25867.93	34972.07	42.52
B800	**1073.00**	60840.00	0.79	9.23	24827.60	24837.62	36002.38	40.82
Assuming 100 °C thermal inertia during pyrolysis								
B500	**773.00**	60840.00	0.79	4.08	28604.39	28609.26	32230.74	47.02
B700	**973.00**	60840.00	0.79	6.57	25859.28	25866.64	34973.36	42.52
B800	**1073.00**	60840.00	0.79	7.86	24827.60	24836.25	36003.75	40.82
Assuming 200 °C thermal inertia during pyrolysis								
B500	**773.00**	60840.00	0.79	2.94	28604.39	28608.12	32231.88	47.02
B700	**973.00**	60840.00	0.79	5.32	25859.28	25865.38	34974.62	42.51
B800	**1073.00**	60840.00	0.79	6.57	24827.60	24834.96	36005.04	40.82

As concurred before, a second case where initial moisture content in CRD wood of 18% (without drying and as received) was also considered, with the assumption of same biochar yields as in the case of pyrolysis with dried CRD wood (Supplementary Table S5). Due to 100-fold increase in biomass water content, $Q_{w,g}$ also increases by the 100-fold margin as pyrolysis temperatures increased from 500-800 °C. The same goes for $Q_{w,v}$ since more energy is wasted to volatilize moisture to steam or vapor. Even then, an increase in Q_{output}, decrease in Q_{net}, and increase in η_{system} this time, it is only due to the higher amount of energy spent to vaporize the 18% water in biomass. At a first glance, this finding seems to be counterintuitive but can be validated by simple thermodynamic concepts coming into play. As much as higher internal moisture content before pyrolysis may have a negative influence in thermal decomposition, its presence up to a certain level is beneficial in some ways. Firstly, this 18% moisture could absorb the heat offered during pyrolysis in a gradual manner, allowing reduced overheating, energy losses (under thermal inertia), and increases Q_{output}. Secondly, the moisture also acts as a thermal buffering agent and stabilizes the system from experiencing excessive heat loss via quick release of pyrolysis gases, thereby, reducing Q_{net}. Lastly, there could be a steady heat transfer amidst the feedstock and within the system that results in better heat management and usage till fruition, increasing overall efficiency.

Supplementary Table S5: Material energy balance and pyrolyzer efficiency during biomass thermal decomposition. Case 2: 18% internal moisture

Horizontal tube furnace reactor with feeding of CRD wood containing 18 wt% initial moisture								
Sample	**Pyrolysis set point temperature (K)**	**Q_{input} (kJ)**	**$Q_{water,vapor}$ (kJ)**	**$Q_{water,gas}$ (kJ)**	**$Q_{biochar}$ (kJ)**	**Q_{output} (kJ)**	**Q_{net} (kJ)**	**η_{system} (%)**
Assuming no thermal inertia during pyrolysis								
B500	**773.00**	4056.00	5.25	35.45	1601.09	1641.78	2414.22	40.48
B700	**973.00**	4056.00	5.25	52.40	1514.65	1572.30	2483.70	38.76
B800	**1073.00**	4056.00	5.25	61.55	1381.63	1448.42	2607.58	35.71
Assuming 100 °C thermal inertia during pyrolysis								
B500	**773.00**	4056.00	5.25	27.18	1601.09	1633.52	2422.48	40.27
B700	**973.00**	4056.00	5.25	43.81	1514.65	1563.71	2492.29	38.55
B800	**1073.00**	4056.00	5.25	52.40	1381.63	1439.28	2616.72	35.49
Assuming 200 °C thermal inertia during pyrolysis								
B500	**773.00**	4056.00	5.25	19.59	1601.09	1625.92	2430.08	40.09
B700	**973.00**	4056.00	5.25	35.45	1514.65	1555.34	2500.66	38.35
B800	**1073.00**	4056.00	5.25	43.81	1381.63	1430.69	2625.31	35.27
Horizontal rotary retort-furnace reactor with feeding of CRD wood containing 18 wt% initial moisture								
Sample	**Pyrolysis set point temperature (K)**	**Q_{input} (KJ)**	**$Q_{water,vapor}$ (kJ)**	**$Q_{water,gas}$ (kJ)**	**$Q_{biochar}$ (kJ)**	**Q_{output} (kJ)**	**Q_{net} (kJ)**	**η_{system} (%)**
Assuming no thermal inertia during pyrolysis								
B500	**773.00**	60840.00	78.75	531.70	28604.39	29214.84	31625.16	48.02
B700	**973.00**	60840.00	78.75	786.00	25859.28	26724.03	34115.97	43.93
B800	**1073.00**	60840.00	78.75	923.19	24827.60	25829.55	35010.45	42.45
Assuming 100 °C thermal inertia during pyrolysis								
B500	**773.00**	60840.00	78.75	407.76	28604.39	29090.91	31749.09	47.82
B700	**973.00**	60840.00	78.75	657.17	25859.28	26595.21	34244.79	43.71
B800	**1073.00**	60840.00	78.75	786.00	24827.60	25692.35	35147.65	42.23
Assuming 200 °C thermal inertia during pyrolysis								
B500	**773.00**	60840.00	78.75	293.78	28604.39	28976.92	31863.08	47.63
B700	**973.00**	60840.00	78.75	531.70	25859.28	26469.73	34370.27	43.51
B800	**1073.00**	60840.00	78.75	657.17	24827.60	25563.53	35276.47	42.02

To sum up, for increasing the efficiency of a pyrolyzer producing biochar as the main product of interest, it needs to operate with a biomass feedstock of low moisture content, small and uniform particle size to avoid heat transfer limitations, and moderate pyrolysis temperature that could conserve yield (high $Q_{biochar}$) as well as curb excessive energy loss while heating steam to reach set point temperatures. As for design optimization, air-tight sealing of entry and exit ports, pre-heating carrier gas, maneuvering rotation speeds in the case of rotary retorts, sheathing ceramic fibers or quartz wool-like material that can offer good insulation around the reactor's body or extremities, and retrofitting heat/biooil/gas/dust recovery and re-usage equipment are immediate suggestions to taper operational costs and maximize energy quality. On a bigger picture, for calculating overall system efficiency, reactor power consumption is also to be included especially when energy integration or re-use (*e.g.:* pyrolysis gas recycling to offset a part of external energy) is under consideration. It is a vital metric for cost analysis and is a huge part of operational expenses determining the system's economic feasibility. Power consumption by auxiliary instrumentation like pumps, cooling, and product recycling systems must also be taken into consideration along with relevant heat losses.

6.4 Methyl orange batch adsorption experiments – An application for CRD wood biochar from the DOE

This section encompasses all theoretical foundations for the adsorption experiments and consists of kinetic, equilibrium, and thermodynamic model equations.

The removal efficiency of B600 adsorbent can be calculated using the expression:

$$\text{Removal efficiency (\%)} = \left(\frac{C_o - C_e}{C_o}\right) \times 100$$

Supplementary Equation S13

Where, C_o and C_e are the initial and equilibrium methyl orange (adsorbate) concentrations in the test solution (mg/L (or) ppm), respectively. The q_e of B600 can be calculated with the equation:

$$q_e\ (mg/g) = \frac{(C_o - C_e)V}{M}$$

Supplementary Equation S14

Where, V is the total volume of the test solution (L) and M is the mass of B600 adsorbent used for the experiment (g).

6.4.1 Adsorption isotherms and effect of initial methyl orange concentrations

Adsorption isotherms typically describe how much of adsorbate is trapped w.r.t to a unit mass of the adsorbent in a given time. For this, 50 mL test solutions with different known concentrations of methyl orange: 8, 30, 40, and 164 ppm, were subjected to adsorption experiments using B600 under the optimal conditions of 50 °C, 24 h (1440 min), pH of 3, and a constant B600 loading of 10 mg/mL (0.5 g/50 mL or 10 g/L). With the resulting C_e and q_e, three models namely, Langmuir, Freundlich, and Temkin isotherms were designed, each highlighting specific adsorption patterns. Upon fitting the experimental adsorption data to these models, adsorption parameters were determined.

6.4.1.1 Langmuir isotherm

Theoretically speaking, Langmuir model states that an adsorbent has specific or finite number of uniform adsorption sites arranged as a single boundary layer with the same binding nature to which the adsorbate firmly attaches to, without any rampant migration from one binding site to another. From [113], the parameter q_e derived from this model can be expressed via a non-linear equation as:

$$q_e = \frac{C_e q_m K_L}{1 + C_e K_L}$$

Supplementary Equation S15

The above equation can be represented in a straight-line format, y=mx+c.

$$\frac{1}{q_e} = \left(\frac{1}{K_L q_m}\right)\frac{1}{C_e} + \frac{1}{q_m}$$

Supplementary Equation S16

Plotting $1/q_e$ versus $1/C_e$ yields a linear plot with an intercept ($1/q_m$) and slope ($1/K_L q_m$) that are used to calculate q_m and K_L. From [121], q_m represents the required adsorbate per unit mass of the adsorbent (mg/g) when monolayer adsorption can be completed to fruition, and K_L denotes the Langmuir isotherm constant describing the affinity between the adsorbate and the adsorbent (L/mg).

In this monolayer adsorption model, a dimensionless separation factor R_L is introduced which is also referred to as the Langmuir isotherm constant [118]. It determines the favourability of the overall adsorption process. By [119], if the condition $0<R_L<1$ is established, the adsorption process is deemed favorable and successful. Secondly, according to [120], if $R_L=0$, the adsorption process is strong and irreversible. Thirdly, if $R_L=1$, the adsorption is linear where the amount of

adsorbate affixed is directly dependent on its initial concentration in the solution [118]. Lastly, when R_L>1, the process is not suitable or is considered unfavourable [20]. R_L can be calculated using the following expression:

$$R_L = \frac{1}{1 + (C_o K_L)}$$

Supplementary Equation S17

In this equation, C_o can be varied to check the influence of initial adsorbate concentration on the adsorption favourability (8, 30, 40, and 164 mg/L in our case).

6.4.1.2 Freundlich isotherm

Freundlich model describes adsorption based on heterogeneous surfaces with non-uniform, active binding sites [72,114]. In this case, more than one layer (multilayer) of adsorbate molecules could stack up over each other reducing the effective binding strength and proximity of these aggregates with the adsorbent. As a result, adsorption may result from weak forces of attraction like intermolecular and Vanderwaals (physisorption) also, aside from stronger chemisorption phenomena [115]. Hence, q_e may directly depend on the concentration of the adsorbate in the solution that will dictate the nature of molecular collisions with biochar (increases the possibility of occupying the active sites faster). Once again, from [113], this model can be viewed non-linearly as:

$$q_e = K_F C_e^{1/n}$$

Supplementary Equation S18

Or, can also be represented as a straight-line equation, yielding a linear plot of $\ln q_e$ versus $\ln C_e$.

$$\ln q_e = \ln K_F + \frac{1}{n} \ln C_e$$

Supplementary Equation S19

Where, K_F [(mg/g)(L/mg)$^{1/n}$] and n are called Freundlich isotherm constants circumventing the adsorption efficiency [16]. The intercept ($\ln K_F$) and slope (1/n) derived from the plot are used to calculate K_F and 1/n, respectively. Higher K_F values denote a higher capacity for adsorption [121]. The constant n on the other hand, indicates the intensity of adsorption. If the condition 0<1/n<1 is obeyed, the process is favourable and multilayer sites develop [116]. If 1/n=1, adsorption is fairly linear and simplified with no exceptional interaction observations of adsorbate over the adsorbent, as stated in [117]. Whereas, if 1/n>1, adsorption becomes unfavourable and the adsorbent's capacity could decline [116].

6.4.1.3 Temkin isotherm

The Temkin model, unlike Langmuir, and similar to Freundlich, delineates that adsorption is non-uniform mainly with an increase in surface occupancy and simultaneous linear decrease in the heat of adsorption [122]. So, different binding sites could operate at specific energy levels (high versus low) and may be dependent on the temperature of the process as well to reduce any activation energy barriers. Temkin isotherm model also hints at a good possibility of multilayer adsorption. The method can non-linearly be expressed as:

$$q_e = \frac{RT}{b_T} \ln(C_e K_T)$$

Supplementary Equation S20

Where, R is the universal gas constant (8.314 J/mol.K), T is the adsorption reaction temperature (323 K), b_T is a Temkin model constant that manifests heat of adsorption process (J/mol) – superimposed by the parameter B, and K_T is an equilibrium constant for binding (L/mg) [131].

A linear representation is yielded from the same equation:

$$q_e = \frac{RT}{b_T}[\ln C_e + \ln K_T]$$

Supplementary Equation S21

For ease of reporting, substituting $\frac{RT}{b_T}$ as B in the above equation, where B represents the change in adsorption heat generated as the adsorbent's surfaces are gradually occupied by the adsorbate (J/mol),

$$q_e = B[\ln C_e + \ln K_T]$$

Supplementary Equation S22

As a straight-line equation, y=mx+c,

$$q_e = B\ln C_e + B\ln K_T$$

Supplementary Equation S23

A plot of q_e versus $\ln C_e$ results in a slope (B) and intercept ($B\ln K_T$) which are used to calculate B and K_T.
As advised in [115], adsorption parameter calculation from these isotherms may experience inaccuracies owing to linearizing the model. Thus, non-linear fitting is also suggested to cross-verify any differences that might occur. However, since our isotherms fit better under linearization, non-linear models are not considered here.

6.4.2 Adsorption kinetics and effect of adsorption duration/time

Kinetic models like pseudo-first order, pseudo-second order, and intra-particle diffusion, can describe the reaction rate and mechanisms of an adsorption system [124]. Pseudo-first and second order models particularly focus on a solid-liquid system where adsorption is directly proportional to the available active adsorption sites along with adsorbate concentration, and the square of these concentrations, respectively. The former supports physisorption due to a weak interactions at the interphase whereas the latter model may also support chemisorption due to strong chemical interactions between molecules of the adsorbate with the adsorbent [69]. Hence, there might be a competition possible in this case for the binding sites where the entity with the strongest binding strength is adsorbed. Hence, the pseudo-second order model will indicate a relatively favourable adsorption [125]. Intra-particle diffusion model on the other hand, discusses the role of adsorbent's porous channels and voids that support binding aside from boundary layer adsorption [126]. The model fit of these methods, help to determine the mechanism of adsorption, how mass transfer occurs, prevalence of diffusion, and any synchronous patterns of adsorption. Upon fitting batch adsorption experimental data to these models, linear and non-linear fitting followed by regression analysis were used to calculate process parameters like q_e, rate constants, and the model fit, R^2. For this, 50 mL test solutions with two different known concentrations of methyl orange: 8 and 164 ppm, were subjected to adsorption experiments using B600 under the optimal conditions of 50 °C, 4 h (240 min), pH of 3, and a constant B600 loading of 10 mg/mL (0.5 g/50 mL or 10 g/L). From [127], the linearized and non-linearized fitting equations as in Supplementary Table S6 can be arrived at!

Supplementary Table S6 : Non-linear and linear fitting equations for adsorption kinetic models

Adsorption kinetic model	Equation	Parameters and significance	Plot axes
Non-linear fitting			
Pseudo-first order	$q_t = q_e\left(1 - e^{-k_1 t}\right)$ **Supplementary Equation S24**	q_e: equilibrium dye adsorption (mg/g); q_t: dye adsorption at time, t (mg/g); k_1: first order rate constant (min^{-1})	q_t (mg/g) on y-axis versus t (min) on x-axis
Pseudo-second order	$q_t = \frac{q_e^2 k_2 t}{1 + q_e k_2 t}$ **Supplementary Equation S25**	q_e: equilibrium dye adsorption (mg/g); q_t: dye adsorption at time, t (mg/g); k_2: second order rate constant (g/mg.min)	q_t (mg/g) on y-axis versus t (min) on x-axis
Linear fitting			
Pseudo-first order	$\ln(q_e - q_t) = \ln q_e - \frac{k_1}{2.303} t$ **Supplementary Equation S26**	q_e: equilibrium dye adsorption (mg/g); q_t: dye adsorption at time, t (mg/g); k_1: first order rate constant (min^{-1})	$Ln(q_e-q_t)$ (mg/g) on y-axis versus t (min) on x-axis
Pseudo-second order	$\frac{t}{q_t} = \frac{1}{k_2 q_e^2} + \frac{1}{q_e} t$ **Supplementary Equation S27**	q_e: equilibrium dye adsorption (mg/g); q_t: dye adsorption at time, t (mg/g); k_2: second order rate constant (g/mg.min)	$\frac{t}{q_t}$ on y-axis versus t (min) on x-axis
Non-linear/linear fitting			
Intra-particle diffusion	$q_t = k_3 t^{1/2} + C$ **Supplementary Equation S28**	q_t: dye adsorption at time, t (mg/g); k_3: intra-particle diffusion constant ($mg.min^{1/2}$); C: constant for solid-liquid interphase (mg/g)	q_t (mg/g) on y-axis versus $t^{1/2}$ (min) on x-axis

For both adsorption kinetics and isotherm evaluation, the comparison between experimental and calculated q_e sheds light on the effectiveness of the study. This was accomplished via the root mean square error (RMSE) and chi-square error (χ^2) tests. The equations can be represented as:

$$\mathrm{RMSE} = \sqrt{\frac{1}{n-1}\sum_{n=1}^{n}(q_{e,exp} - q_{e,cal})^2}$$

Supplementary Equation S29

$$\chi^2 = \sum \frac{(q_{e,exp} - q_{e,cal})^2}{q_{e,cal}}$$

Supplementary Equation S30

Where, n is the number of data points considered, $q_{e,exp}$ and $q_{e,cal}$ are the equilibrium adsorption capacities from experimental investigations and from fitting with the theoretical models (calculated), respectively. The closer the values are to '0', the more reliable an adsorption model is!

6.4.3 Adsorption thermodynamics

Thermodynamic parameters indicate if an adsorption phenomenon is occurring with feasibility, hints at the requirements of external energy, and the degree of randomness. Almost the same batch adsorption conditions as followed for kinetics was applied, only difference being the ramping up of temperature from 20-50 °C. The calculations were performed only for the initial methyl orange concentration of 8 ppm as an example. C_e and q_e are calculated once again, which eventually determine the distribution or partition coefficient, k_d (L/g) [132]:

$$K_d = \frac{q_e}{C_e}$$

Supplementary Equation S31

Then, the thermodynamic parameters such as enthalpy (**ΔH:** KJ/mol), entropy (**ΔS:** KJ/mol), and Gibbs free energy (**ΔG:** KJ/mol.K) were analyzed to seek insights on the nature of adsorption processes and link it with the effect of rising temperatures. These can be quantified as follows [133]:

$$\ln K_d = \frac{\Delta S}{R} - \frac{\Delta H}{RT}$$

Supplementary Equation S32

where, R is the universal gas constant (8.314 J/mol.K) and T is the absolute or reaction temperature (293-323 K). Viewing the aforementioned expression as a straight-line equation, plotting $\ln k_d$ versus 1/T yields a slope (-ΔH/R) and an intercept ΔS/R. With this, ΔG can be calculated from either [95]:

$$\Delta G = \Delta H - T\Delta S$$

Supplementary Equation S33

Or, from the equation mentioned in [132]

$$\Delta G = -RT\ln K_d$$

Supplementary Equation S34

6.4.4 Other relevant biochar-methyl orange adsorption studies

Supplementary Table S7: Comparison of methyl orange removal by biochars from relevant studies

Biomass source for biochar	Surface area (m^2/g)	q_e (mg/g)	Temperature of adsorption (°C)	pH of adsorption	Time of adsorption (min)	Adsorbent dosage (g or g/L)	Dye removal efficiency (%)	Reference
Lemon peel	111.45	17.21	25	4	60	0.025	90.87	**[128]**
Waste antibiotic fermentation residue	1269	521.03	25	3-9	240	0.25-0.50	69.84-90.18	**[22]**
Delonix regia seed pods	8.36-15.39	144.9	25	1.01	150	0.75-1	97.95	**[107,108]**
Wheat straw	747.76-2578.82	93.98-119.76	25	2 (6)[*1]	15-30	0.002-0.014	90-95	**[111]**
Prosopis juliflora	1.28	8.31	25	6	15[*2]	0.1	64	**[131]**
Palmer Amaranth (invasive weed)	19.6	495.0-554.3	25-45	4	120-240	0.020-0.5	95-100	**[100]**
Hyphaene thebaica	33.38	264.92	40	2	10-20	0.03	---	**[121]**
Poultry manure	16.09	20.8	25	4	80[*3]	2.5	88.80	**[97]**

Rice husk	115.59	31.63	25	3	240	0.2	---	**[99]**
Date palm fronds	431.82	163.13	25	4	0-1180[*4]	0.002-0.020	---	**[138]**
Birch wood	437.34	220	20	2	<1020	0.5-2.5	---	**[16]**
Ayurvedic waste-iron oxide composite	151.15-398.39	33.90	44	3	60	4	100	**[20]**
CRD wood	323.78	14.63	50	3	<1440	10	89-99	**This work**

[*1] – Adsorption of methyl orange was greater than 90% and ideal till a pH of 6. The adsorption behaviour could also be linked to the molar ratio of chemical activation agent since porosity and surface area of resulting biochar increased till an impregnation ratio of 1:1 (biomass:KOH).

[*2] – Saturation was seen around 15 min, methyl orange removal efficiency was tested till 40 min

[*3] – Maximum adsorption seen at or within 120 min after which saturation was observed

[*4] – First phase within 60 min showed maximum adsorption followed by a slow second phase till 360 min, and then saturation